01 Sep 2008

Discrete-Time Ripple Correlation Control for Maximum Power Point Tracking

Jonathan W. Kimball
Missouri University of Science and Technology, kimballjw@mst.edu

Philip T. Krein

Recommended Citation

J. W. Kimball and P. T. Krein, "Discrete-Time Ripple Correlation Control for Maximum Power Point Tracking," *IEEE Transactions on Power Electronics*, vol. 23, no. 5, pp. 2353-2362, Institute of Electrical and Electronics Engineers (IEEE), Sep 2008.
The definitive version is available at https://doi.org/10.1109/TPEL.2008.2001913

Discrete-Time Ripple Correlation Control for Maximum Power Point Tracking

Jonathan W. Kimball and Philip T. Krein

***Abstract*—Ripple correlation control (RCC) is a high-performance real-time optimization technique that has been applied to photovoltaic maximum power point tracking. This paper extends the previous analog technique to the digital domain. The proposed digital implementation is less expensive, more flexible, and more robust. With a few simplifications, the RCC method is reduced to a sampling problem; that is, if the appropriate variables are sampled at the correct times, the discrete-time RCC (DRCC) algorithm can quickly find the optimal operating point. First, the general DRCC method is derived and stability is proven. Then, DRCC is applied to the photovoltaic maximum power point tracking problem. Experimental results verify tracking accuracy greater than 98% with an update rate greater than 1 kHz.**

***Index Terms*—Maximum power point tracking (MPPT), optimization, photovoltaic (PV).**

NOMENCLATURE

φ	Equilibrium value of a variable z.
φ^*	Value of z that corresponds to a cost function optimum J^*.
ψ	Zero-average ripple on x.
C	Small-signal capacitance of photovoltaic (PV) panel.
D	Duty ratio.
f	Time derivative of z.
i_{panel}	PV panel current.
J	Generic cost function.
J^*	Optimal value of J.
k, $\hat{k}$	Control gain.
k_{CVF}	Approximate ratio between PV panel voltage at maximum power and V_{oc}.
n	Number of switching periods between samples.
p_{panel}	PV panel power.
q	Switching function (binary-valued).
R	Small-signal resistance of PV panel.
t_0	Previous instant of control adjustment.
t_{sample}	Sampling instant (time within period).
T	Period of ripple on x.
u	Generic control input.
v_{panel}	PV panel voltage.
V_{oc}	PV panel open-circuit voltage.
w_+	Positive slope of z.
w_-	Negative slope of z.
x	Variable that has ripple.
z	Generic correlation variable.

Manuscript received March 17, 2008; revised May 28, 2008. Current version published November 21, 2008Recommended by Associate Editor K. Ngo.

J. W. Kimball is with the Missouri University of Science and Technology, Rolla, MO 65409 USA (e-mail: kimballjw@mst.edu).

P. T. Krein is with the University of Illinois at Urbana-Champaign, Urbana, IL 61801 USA (e-mail: krein@illinois.edu).

Digital Object Identifier 10.1109/TPEL.2008.2001913

I. INTRODUCTION

POWER electronics applications provide ample opportunities for energy-based optimization. Induction motor flux magnitude [1]–[7] or dc-dc converter deadtime [8], [9] can be adjusted for maximum efficiency. Active filters can be tuned for best performance [10]. Most alternative energy sources have a well-defined operating point where they deliver either maximum power or maximum efficiency. In particular, photovoltaic (PV) cells should always be operated at their maximum power point, a task accomplished by a maximum power point tracking (MPPT) control. Many MPPT methods of varying complexity have been proposed in both analog and digital frameworks [11].

Ripple correlation control (RCC) [12]–[14] is a real-time optimization method particularly suited for switching power converters. Its objective is to maximize or minimize a cost function, such as a power or energy quantity in an MPPT application. RCC uses information present in the inherent switching ripple to determine the gradient of the cost function. The result is that information available on the fast time scale of current and voltage ripple enables the control to attain a slow time scale objective, operation at the optimum. RCC has been applied to the MPPT problem [12]–[21], motor efficiency maximization [12], [22]–[27], deadtime optimization [12], [28], [29], and filter tuning [10].

Discrete-time ripple correlation control (DRCC) extends RCC to the discrete-time domain [30], [31]. A brief summary of RCC is included in Section II for background. In principle, the RCC signals could be sampled at a high rate and the continuous-time method could be transformed to discrete time. This requires sampling at many times the switching frequency, and has limited practical merit. Instead, knowledge of waveshapes can be used to drastically reduce the sampling requirements

while achieving equivalent results, as shown in Section III. Section IV proves that the algorithm has a steady-state equilibrium where the ripple encircles the maximum power point. Section V introduces a mode-switching algorithm in the context of an experimental MPPT that helps ensure global optimization rather than the local optimum operation typical of most gradient controls. An experimental converter achieves greater than 98% tracking accuracy in direct sun at update rates of 1 kHz or more.

II. Background: Ripple Correlation Control

RCC uses switching ripple to optimize a cost function J that is a function of a state variable z. The experimental converter described in Section V is applied to an MPPT application for a PV panel, so the development in Sections II–IV will assume that the objective is to choose a cost function representative of panel power and maximize J. An equivalent formulation can be developed to minimize a cost function, as in efficiency maximization (power loss minimization), with a sign change. Global stability requires that J is unimodal, that is, there is a single global maximum. In a practical solar application, local shading can create multiple peaks [32], and the mode-switching method of Section V can increase the likelihood that the global maximum is achieved.

For a suitable cost function $J(z)$, the maximum value occurs where

$$\frac{dJ}{dz} = 0. \tag{1}$$

The power conversion plant has an input u (such as the duty ratio in a dc-dc converter). Just as J must be unimodal, the steady-state value

$$\varphi(u) = \lim_{t\to\infty} z(u,t) \tag{2}$$

must be monotonic over the operating range. Monotonicity ensures that there is no polarity inversion in the system gain, and may be satisfied by limits on u or by a coordinate transformation. An integral control law

$$u = k\int \frac{dJ}{dz}dt \tag{3}$$

will drive the operating point to the maximum value of J. The sign of k and the effect of u on z determine whether the control law goes towards a maximum or a minimum. The magnitude of k influences convergence rate.

Usually, derivatives like dJ/dz are unavailable in a practical system, so a more useful controller is needed. If the integrand of (3) is multiplied by a positive value, the equilibrium operating point does not change. A convenient multiplier is $(dz/dt)^2$, which by the chain rule yields

$$u = k\int \frac{dJ}{dz}\frac{dz}{dt}\frac{dz}{dt}dt = k\int \frac{dJ}{dt}\frac{dz}{dt}dt. \tag{4}$$

This control law only needs time derivatives, likely to be readily available in a real system. The transformation is possible if dz/dt is nonzero, except at isolated points that will not contribute to the integral. In particular, if the converter is always switching with a duty ratio $D \in (0,1)$ and switching period $T > 0$, then the derivatives of state variables such as currents and voltages will in fact be nonzero except at switching edges, and provide suitable choices for z.

Many approximations to (4) have been suggested, all of which require at least one multiplication. Often in dc-dc converters, dz/dt is piecewise constant. If the sign information is adequate, then a synchronous demodulator can be used. In this approach [20], [28], [29], J is calculated (usually with a multiplication), dJ/dt is determined with a filter, and analog switches controlled by $\mathrm{sgn}(dz/dt)$ determine an integrand similar to (4). Another variation is to consider only the phase information [10], [33]. In this formulation, RCC resembles a phase-locked loop. In principle, the two simplifications can be combined, where the integrand is approximated as $\mathrm{sgn}(dJ/dt)\mathrm{sgn}(dz/dt)$. These approximations affect noise immunity, convergence rate, and potentially the equilibrium value, since some information has been discarded.

RCC to date has been implemented with analog circuits. Time derivatives can be obtained easily. To achieve better noise immunity, though, the derivative function usually is replaced with a filter whose gain rolls off well above the frequency range of interest, which is normally around the switching frequency. Multiplication is possible with an analog multiplier such as an AD633. Unfortunately, typical analog multipliers are implemented in bipolar technology and have relatively high bias currents. For example, an Analog Devices AD633 consumes 120 mW under rated conditions.

RCC is a general-purpose optimization technique for real-time applications. As long as states and cost functions that both contain ripple can be identified, there will be adequate information to find the optimum operating point. RCC is particularly well-suited to switching power converters, since the switching action continuously excites the states and creates ripple. RCC has also been proposed for motor drive applications. The stored energy in the motor's magnetic field may damp out the ripple that results from the main switching elements. In this case, an extra ripple term at a suitable low frequency can be added to produce the necessary nonzero dz/dt signal. Other observer-based solutions that provide signals for the RCC control law are likely to be possible.

III. Discrete-Time Formulation

A digital version of RCC is preferable for many reasons. While analog multipliers tend to be power-hungry, low-power microcontrollers are available with hardware digital multipliers. For example, an MSP430F148 has a hardware 8×8 bit multiplier, and the total microprocessor core consumes less than 2.5 mW. A digital implementation enables other features, too, such as protection modes and user interfaces.

While the analog control law (4) could be converted to discrete-time with fast sampling, e.g., ten or more samples per switching period, and a suitable high-end microcontroller or DSP, the application of general waveform knowledge yields a simpler control law. In dc-dc converter applications, z is piecewise linear, so its time derivative is piecewise constant: first a

positive value w_+, then a negative value w_-. Over a time interval from 0 to T

$$\dot{z} = \begin{cases} w_+, & \mathrm{mod}(t,T) \in [0, DT) \\ w_-, & \mathrm{mod}(t,T) \in [DT, T). \end{cases} \tag{5}$$

Here, T is the switching period and D is the fraction of the period when $\dot{z} > 0$, which may or may not be the same as the duty ratio of a controlled switch. Both D and T may vary, so long as neither goes to zero and D does not go to 1. The form for $\dot{z}$ in (5) can be substituted into (4). A definite integral determines the change in u over a single period. The period can be subdivided according to the value of $\dot{z}$ and the definite integral can be evaluated symbolically

$$\begin{aligned} u(T) &= u(0) + kw_+ \int_0^{DT} \dot{J} dt + kw_- \int_{DT}^{T} \dot{J} dt \\ u(T) &= u(0) + kw_+ \left[J(DT) - J(0) \right] \\ &\quad + kw_- \left[J(T) - J(DT) \right]. \end{aligned} \tag{6}$$

This result (6) can be generalized to any switching period that is aligned with the minimum of z (the rising edge of $\dot{z}$). If a periodic steady-state condition is possible, it would require

$$\begin{aligned} J(0) &= J(T) \\ w_+ D + w_-(1-D) &= 0. \end{aligned} \tag{7}$$

These relationships (7) can be substituted into (6) to give a control law of

$$u(T) = u(0) + \frac{kw_+}{1-D} \left(J(DT) - J(0) \right). \tag{8}$$

Just as many approximations have been proposed for the analog RCC law (4), there are possible simplifications for (8). Instead of using a gain on the difference between samples of J, use a gain on the sign of the difference. If the actuation is quantized, there may be no practical difference between (8) and

$$u(T) = u(0) + \hat{k} \mathrm{sgn} \left(J(DT) - J(0) \right). \tag{9}$$

Thus, the input is adjusted in proportion to the sign of the difference between two samples. In periodic steady state, not only will $J(T) = J(0)$ and $u(T) = u(0)$, but also notice that the process will drive J to its optimum and will produce $J(DT) = J(0) = J(T)$. The control law of (9) is related to delta modulation [34]. A generalization is to hold u constant for several cycles nT, then update u based on two samples within a single cycle. The experimental system discussed below uses a controller of the form

$$\begin{aligned} u(t_0 + nT) = u(t_0) + \hat{k} \mathrm{sgn} \big(& J\left(t_0 + (n - 1 + D)T\right) \\ & - J\left(t_0 + (n-1)T\right) \big) \end{aligned} \tag{10}$$

with $n = 20$ to yield low control power.

The key result of this analysis is that all of the information needed to drive the operating point to its optimum can be obtained from two samples per switching period, taken at specific times: when the state variable z is at a maximum and when z is at a minimum. At equilibrium, J oscillates around the maximum at twice the switching frequency and reaches the same value at each end of the oscillation.

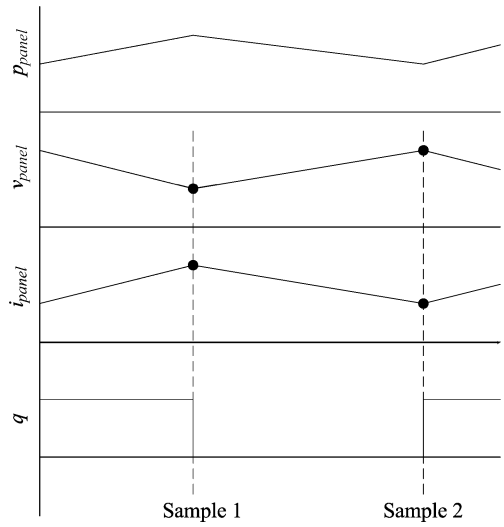

Fig. 1. Samples away from maximum power point (current is too low).

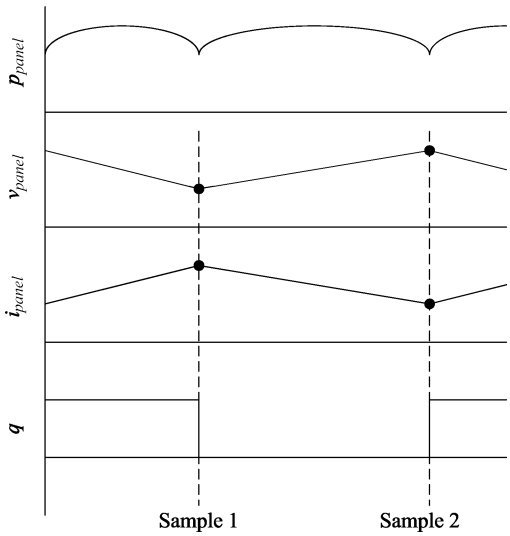

Fig. 2. Samples at the maximum power point.

The sampling process is shown in Figs. 1 and 2 for an MPPT. The generic cost function J is implemented as p_{panel}, the panel power. The state variable z is chosen as i_{panel}, the panel current. Panel voltage v_{panel} is also sampled to allow computation of $p_{\mathrm{panel}} = v_{\mathrm{panel}} i_{\mathrm{panel}}$. In Fig. 1, the panel is not at the maximum power point—current needs to increase. In Fig. 2, the panel is at the maximum power point. The instantaneous power passes through the maximum twice in each switching cycle, once while the current is increasing and once while the current is decreasing. The average delivered power is essentially as high as possible in Fig. 2, limited only by the converter ripple. The control algorithm is shown in block diagram form in Fig. 3.

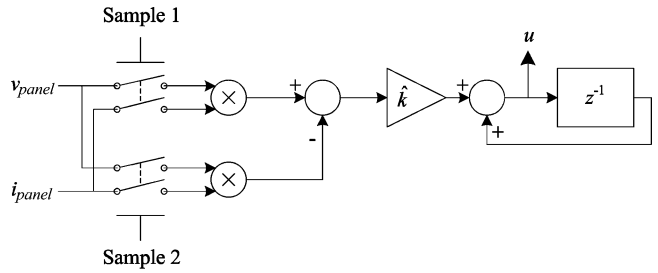

Fig. 3. Block diagram of DRCC sampling process.

Although the DRCC control law (10) superficially resembles a conventional perturb-and-observe (P&O) process for optimum tracking [35], there are at least two primary differences. First, the time scale is far different. The P&O technique uses two samples of output power that correspond to two steady-state operating points. When the operating point is adjusted under a P&O method, the system must wait for all transients to settle before recording information. In contrast, DRCC uses a pair of samples within a single switching period. The update rate can be as fast as the switching frequency, with suitable choices of the microcontroller and analog-to-digital converter (ADC) system. Second, P&O always leaves the present operating point to determine whether the optimum is nearby. It does not fully converge, in the sense that the operating point must be adjusted on a continuing basis. DRCC uses information in the ripple at a given operating point to determine whether equilibrium has been reached, and will in fact converge to a specific duty ratio, altering it automatically if a parameter changes. P&O always exhibits subharmonics (large-signal operating point ripple at a fraction of the MPPT update rate), whereas DRCC achieves true equilibrium.

IV. DRCC Stability

The stability of continuous-time RCC was proven in [22], but a new stability proof is needed for the much simpler DRCC process. There are two aspects to prove: first, that the equilibrium corresponds to the optimum, and second, that the control law (10) will cause the operating point to converge to this equilibrium. The proof below will consider only the maximization problem, since minimization can be achieved with a sign change on the gain k.

A few assumptions and definitions are necessary. Assume that the plant has an average model

$$\frac{dz}{dt} = f(z, u). \tag{11}$$

The average-model state variable z can be related to the physical state variable x with an algebraic ripple correction function ψ

$$x(t) = z(t) + \psi(u, t). \tag{12}$$

Although the variable names and terminology are different, this is the same concept as in Krylov–Bogoliubov–Mitropolsky (KBM) averaging [36], [37]. The ripple ψ is small (relative to x and z) with zero mean over a switching period. Assume also that the dynamical system (11) has an equilibrium at $z = \varphi(u)$. The input is constrained such that

$$u \in [u_{\min}, u_{\max}]. \tag{13}$$

The equilibrium function $\varphi(u)$ must be monotonic on this interval. The cost function $J(z)$ is assumed to be unimodal, with a unique maximum

$$\max_{u\in[u_{\min},u_{\max}]} J(\varphi(u)) = J(\varphi*) = J*. \tag{14}$$

Equilibrium is reached where the control law (10) causes no change in u from sample to sample. The input u is updated every nT based on two samples of J during the immediately preceding switching interval. By the definition of duty ratio, the change in u is

$$\hat{k}\operatorname{sgn}\left[J\left(z + \min_{t\in[(n-1)T,nT]}\psi(u,t)\right) - J\left(z + \max_{t\in[(n-1)T,nT]}\psi(u,t)\right)\right]. \tag{15}$$

If nT is sufficiently large, $z \approx \varphi(u)$. Rolle's theorem states (as quoted from [38, p. 154]):

> Suppose f is continuous on the interval $[a, b]$ and differentiable on (a, b). If $f(a) = f(b)$, then there exists at least one number $c, a < c < b$, with $f'(c) = 0$.

This applies to DRCC directly. Equilibrium corresponds to a point where u no longer changes, which means that the two samples of J are equal. To restate Rolle's theorem in the appropriate variables:

> Suppose J is continuous on the interval

$$\left[\varphi(u(t_0)) + \min_{t\in[(n-1)T,nT]}\psi(u(t_0),t),\ \varphi(u(t_0)) + \max_{t\in[(n-1)T,nT]}\psi(u(t_0),t)\right] \tag{16}$$

> and differentiable on the corresponding open interval. If

$$J\left(\varphi(u(t_0)) + \min_{t\in[(n-1)T,nT]}\psi(u(t_0),t)\right) = J\left(\varphi(u(t_0)) + \max_{t\in[(n-1)T,nT]}\psi(u(t_0),t)\right) \tag{17}$$

> then there is at least one number φ^* in the interval (16) with

$$\frac{dJ}{dz}(\varphi*) = 0. \tag{18}$$

So, the equilibrium occurs where the ripple band encloses the maximum. This is as close to the maximum as any sample-based control law can reach without full knowledge of the plant dynamics. The ripple band can be made arbitrarily small through design choices that trade tracking accuracy, switching frequency, and signal-to-noise ratio.

Since the equilibrium is the correct operating point, the next objective is to prove that the control law (10) will converge to the equilibrium. Define

$$\begin{aligned}\Delta J &= J\left[\varphi\left(u(t_0+nT)\right)\right] - J\left[\varphi\left(u(t_0)\right)\right]\\ \Delta\varphi &= \varphi\left(u(t_0+nT)\right) - \varphi\left(u(t_0)\right)\\ \Delta u &= u(t_0+nT) - u(t_0).\end{aligned} \tag{19}$$

The third new variable Δu is determined by (10). For sufficiently small Δu

$$\begin{aligned}\Delta J &= \Delta\varphi \times \frac{dJ}{d\varphi}\left[\varphi\left(u(t_0)\right)\right]\\ \Delta\varphi &= \Delta u \times \frac{d\varphi}{du}\left(u(t_0)\right).\end{aligned} \tag{20}$$

Two derivatives are needed in (20). For sufficiently small ripple, see (21) shown at the bottom of the page. That is, the derivative is approximated by the difference in two samples of J divided by the difference in the corresponding values of x. The other derivative $d\varphi/du$ is known to be of constant sign since $\varphi(u)$ is monotonic. Through a series of substitutions, we find (22), shown at the bottom of the page.

There are four factors in (22). The derivative $d\varphi/du$ is of constant sign because of monotonicity. The absolute value in the numerator results from multiplying the actual difference by the sign of the difference. The denominator is always negative, as the difference between a minimum and a maximum. The gain $\hat{k}$ is constant and can be chosen so that ΔJ is always positive (approaching the desired operating point) or zero (at equilibrium). The sign of the gain must be

$$\operatorname{sgn}\hat{k} = -\operatorname{sgn}\frac{d\varphi}{du}. \tag{23}$$

The magnitude of the gain is chosen for a particular problem so that the system quickly approaches the maximum without undue overshoot. Conceptually, this is similar to Newton's method or, more precisely, the secant method [39]. A large gain will cause oscillation around the maximum, while a small gain will slowly traverse J until reaching equilibrium.

So as long as the physical plant satisfies some basic conditions—unimodal $J(z)$, monotonic $\varphi(u)$—the DRCC control law (10) will force the plant to converge to the equilibrium where $J(z)$ is maximized. The control designer must choose an appropriate cost function, an appropriate correlation variable z, and the gain $\hat{k}$. As was shown in [21], z must be chosen to minimize phase delay effects in the system. That is, most practical systems have more than one state variable. The problem must be reformulated into a scalar system that most nearly approximates the real system in the frequency range of interest. For a PV MPPT, the best solution is to choose the right physical variable, usually panel voltage. For other systems, observers and state coordinate transformations may be helpful.

V. Application to Solar Power

RCC has been explored in detail for PV maximum power point tracking [15]–[18], [21], the application that motivated the present work. RCC-based MPPT controls are extremely fast and accurate. DRCC retains these characteristics and offers several advantages over RCC, such as low power consumption due to digital implementation and inherent simplicity.

PV panels deliver maximum power at a particular operating point that varies with insolation and temperature. A typical I-V characteristic for a solar cell is

$$i_{\text{panel}}(v_{\text{panel}}) = I_{\text{SC}}\left(1 - \exp\left(\frac{v_{\text{panel}}}{mV_T}\right)\right). \tag{24}$$

I_{SC} is the short-circuit current, which varies linearly with the insolation. V_T is the thermal voltage (kT/q) and m is a technology-dependent scale factor. The voltage on a PV panel scales with the number of cells connected in series, while the current is limited by the weakest cell in a series string (to a first approximation). Power, the product of current and voltage, has a well-defined maximum where current is a large fraction of I_{SC} and voltage is a large fraction of the open-circuit voltage V_{OC}. Experimental results for panel current and power, as functions of voltage, are shown in Fig. 4 for the panel used in the experiments to follow. Notice that the peak power occurs at a panel voltage of about 17 V, compared to an open-circuit voltage of

$$\frac{dJ}{d\varphi}\left[\varphi\left(u(t_0)\right)\right] \approx \frac{J\left[\varphi\left(u(t_0)\right) + \min\limits_{t\in[(n-1)T,nT]}\psi(u,t)\right] - J\left[\varphi\left(u(t_0)\right) + \max\limits_{t\in[(n-1)T,nT]}\psi(u,t)\right]}{\min\limits_{t\in[(n-1)T,nT]}\psi(u,t) - \max\limits_{t\in[(n-1)T,nT]}\psi(u,t)} \tag{21}$$

$$\Delta J = \hat{k}\frac{d\varphi}{du}\left(u(t_0)\right)\frac{\left|J\left[\varphi\left(u(t_0)\right) + \min\limits_{t\in[(n-1)T,nT]}\psi(u,t)\right] - J\left[\varphi\left(u(t_0)\right) + \max\limits_{t\in[(n-1)T,nT]}\psi(u,t)\right]\right|}{\min\limits_{t\in[(n-1)T,nT]}\psi(u,t) - \max\limits_{t\in[(n-1)T,nT]}\psi(u,t)} \tag{22}$$

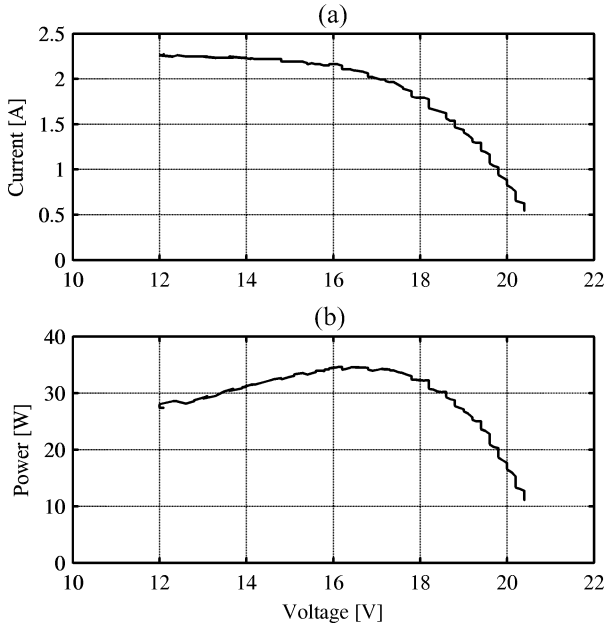

Fig. 4. Panel current and power as functions of voltage.

about 20.5 V. See Section V-B for more details. This shape is typical for all p-n junction PV cells.

DRCC can be used as part of a highly effective MPPT. MPPTs are used to operate a PV panel as close to the maximum power point as possible [11]. For the generic cost function J, an MPPT uses panel power $p_{\rm panel}$. For the correlation variable z, an MPPT can use either panel current $i_{\rm panel}$ or panel voltage $v_{\rm panel}$ or both. As shown in [17] and [21], RCC performs better if voltage is used rather than current. In essence, correlation with $v_{\rm panel}$ reduces the influence of capacitive stored energy on the optimization.

A. Energy Storage Effects

Since the cost function is power, stored energy can affect the performance of DRCC. A PV cell is an illuminated p-n junction, and stores energy in the form of stored charge that varies with voltage. This can be modeled as a nonlinear junction capacitance. A typical MPPT uses a boost converter or other current-fed switching power converter. Panel current then has a predominantly dc value with small triangular ac ripple at the switching frequency. The relationship between ripple current and changes in stored charge (capacitive voltage ripple) varies with the switching frequency. While the ripple current and voltage still contain information about the operating point, the capacitive phase shift complicates the process. The $v_{\rm panel}i_{\rm panel}$ product is not the true panel power, and no longer are voltage and current edges aligned as in Figs. 1 and 2. More realistic waveforms are shown in Fig. 5.

The edges of $di_{\rm panel}/dt$ are exactly aligned with the switching function q, so

$$\operatorname{sgn}\frac{di}{dt} = 2q - 1. \tag{25}$$

The microcontroller which generates the switching waveforms could easily generate sampling signals that are aligned with $di_{\rm panel}/dt$. However, the DRCC algorithm will continue to be

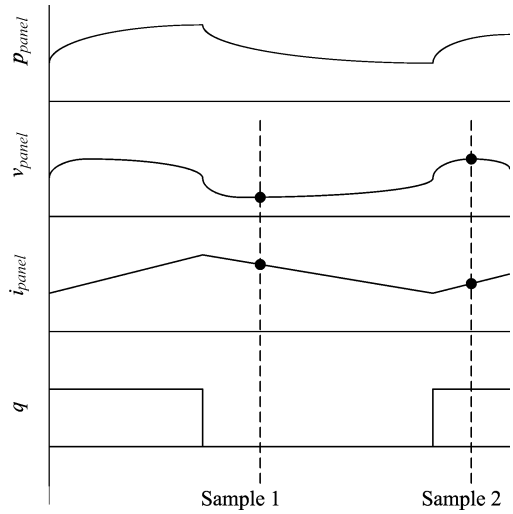

Fig. 5. Sample timing with panel capacitance effects.

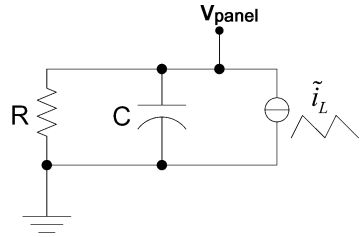

Fig. 6. Small-signal equivalent circuit of solar panel connected to a boost converter.

effective at a much higher switching frequency if samples are aligned with edges of $dv_{\rm panel}/dt$ instead.

A study of the small-signal circuit shown in Fig. 6 reveals the relationship needed to generate sampling signals aligned with edges in $dv_{\rm panel}/dt$. The resistance R in Fig. 6 represents the incremental resistance of the panel (the reciprocal of the slope of the I-V curve shown in Fig. 4). Capacitance increases with voltage while incremental resistance decreases [40]. Over a broad range near the maximum power point, the panel time constant RC is nearly constant. Mono- and polycrystalline silicon panels have been measured in various operating conditions to have a time constant of about 17 μs.

The applied current in Fig. 6 is triangular with a duty ratio governed by the switching waveform q. The appropriate sample time is when

$$\frac{dv_{\rm panel}}{dt}(t_{sample}) = 0. \tag{26}$$

A solution of the differential equation that governs the circuit of Fig. 6 gives a sample time of

$$t_{\rm sample} = DT + RC\ln\left(\frac{1-\exp\left(\frac{(1-D)T}{RC}\right)}{(1-D)\left(1-\exp\left(\frac{T}{RC}\right)\right)}\right). \tag{27}$$

That is, if time is reset to zero at the rising edge of q, the next sample should occur not at DT (the falling edge of q) but rather at $t_{\rm sample}$. Similarly, if time is reset at the falling edge of q, replace D with $(1-D)$ everywhere in (27) to find the sample

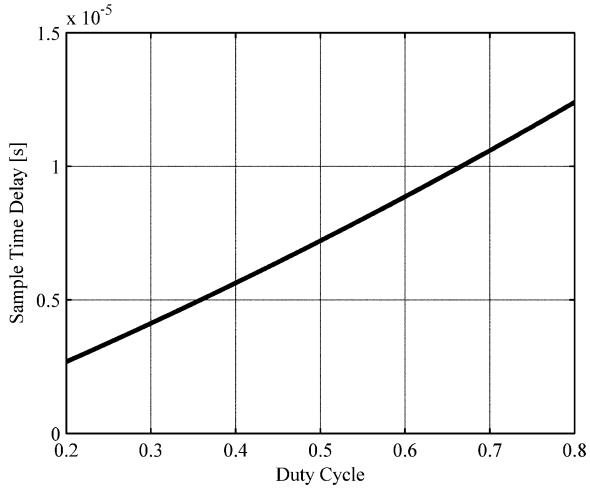

Fig. 7. Sample time delay as a function of duty ratio.

time that occurs after the next rising edge of q. Since the circuit is small-signal and linear, one equation determines the appropriate delay so that all samples align with the edges of (dv/dt).

Equation (27) is too complicated for real-time calculation in an inexpensive 8- or 16-bit microcontroller. Math operations include exponentials, a division, and a natural logarithm. Instead, a linear fit is adequate. Fig. 7 shows a plot of (27) for $RC = 17\ \mu$s and $T = 40\ \mu$s. For the experimental system, a piecewise linear fit was used. Maximum error on the timing was less than 2%, and the corresponding MPPT error was lower.

B. Implementation and Mode-Switching

An experimental MPPT system was built to demonstrate the effectiveness of DRCC. The MPPT employed a boost converter with a 2.6-mH powdered-iron inductor, an IRF3710 MOSFET, and a MBR1545CT Schottky diode. The solar panel was a SolarWorld SW50 mono/RD094, with sample terminal characteristics shown in Fig. 4. The panel is rated for 50 W maximum output, 21.0 V open-circuit voltage, 3.40 A short-circuit current, and maximum power point at 16.7 V and 2.99 A. The switching frequency was set to 25 kHz, a compromise between component sizes and detectable ripple. At lower frequencies, inductor size would be excessive, while at higher frequencies, panel capacitance would attenuate and phase-shift voltage ripple measurements. The DRCC algorithm was executed every 20 switching cycles for low ADC power consumption.

The algorithm was implemented on an MSP430F148. The MSP430 family from Texas Instruments has a 16-bit fixed-point core and a variety of peripherals. The primary advantage of this family is low power consumption, which enables an effective MPPT for a relatively small panel. The MSP430F148 has a hardware 8-bit-by-8-bit (8×8) multiplier, a 12-bit ADC, and several timer channels that can implement pulse-width modulation. Typical power consumption, including peripherals, is 3.6 mW with a nominal 3-V supply.

Voltage and current ripple are only a few percent of the average voltage and current. To achieve high signal integrity and sufficient ADC resolution, each signal was split into a dc component and an ac component. The gains on the ac components of voltage and current were 3.33 times greater and 32 times greater, respectively, than the gains on the dc components. Sampling was performed with 74HC4066 switches. Current was sensed with a LEM LA55-P closed-loop Hall effect sensor with five primary turns, though a commercial implementation would likely use a current shunt instead. With this gain and filter configuration, SNR at the ADC inputs was increased by 10 dB for voltage ripple and 30 dB for current ripple.

As in any gradient-based optimization approach, DRCC drives the system to a local optimum. A mode-switching algorithm was implemented to improve robustness and overall performance over the full range of possible operating conditions. For example, $\varphi(u)$ becomes nearly flat near short-circuit of the solar panel, making its monotonicity sensitive to noise. Multiple maxima of $J(z)$ can occur near open-circuit when several cells are connected in series, particularly under partial shading conditions [32]. Mode switching uses a simple open-loop control to set up an initial condition near the desired operating point to achieve global stability at the optimum.

Here, the other mode (besides DRCC) employs the well-known fractional open-circuit voltage (fractional $V_{\rm oc}$) approach, also referred to as constant voltage fraction (CVF) [41] power tracking. This approximate MPPT technique is ideal for augmenting DRCC. Over a broad range of operating conditions, the maximum power point occurs near a characteristic fraction $k_{\rm CVF}$ of the open-circuit voltage $V_{\rm oc}$. More recent work [42] has shown that a variable fraction achieves higher accuracy. Another option is to employ a fractional short-circuit current approach (fractional $I_{\rm SC}$), which was shown in [39] to be more accurate than fractional $V_{\rm OC}$. In the present application, the objective is to initialize DRCC within the basin of attraction of the true maximum power point, so the simple CVF technique is suitable. Once initialized, the control is turned over to the DRCC process to drive operation to the exact maximum. Use of a sampled $V_{\rm oc}$, rather than a fixed voltage, compensates for temperature variation and panel aging.

The complete algorithm has the following two modes.

1) The CVF process is implemented: the converter is turned off for a brief predetermined time sufficient for the panel to reach $V_{\rm oc}$. At the end of this time, $V_{\rm oc}$ is sampled. Then the converter is set for the specified voltage fraction and driven to a target panel voltage $k_{\rm CVF}V_{\rm oc}$.
2) The DRCC algorithm is enabled. Since the initial conditions are near the maximum power point, convergence is quick (on the order of 10 ms).

In principle, the mode-switching technique can be a one-time event: DRCC will continue to operate at the maximum once initialized, and can easily track changes in conditions even on millisecond time scales. In practice, there is an advantage to having the sequence repeat after a predetermined time, in case large charges in operating conditions have occurred. In the experimental system, the CVF time is 240 ms, including 10 ms for the open-circuit measurement. The DRCC control mode is then activated; the panel reaches the maximum power point in about 10 ms, and the controller continues to track for about 3 s before re-initializing with the CVF mode. The CVF time could be shortened, as long as the time is sufficient for the panel to reach steady-state. The DRCC time could be extended to minutes or

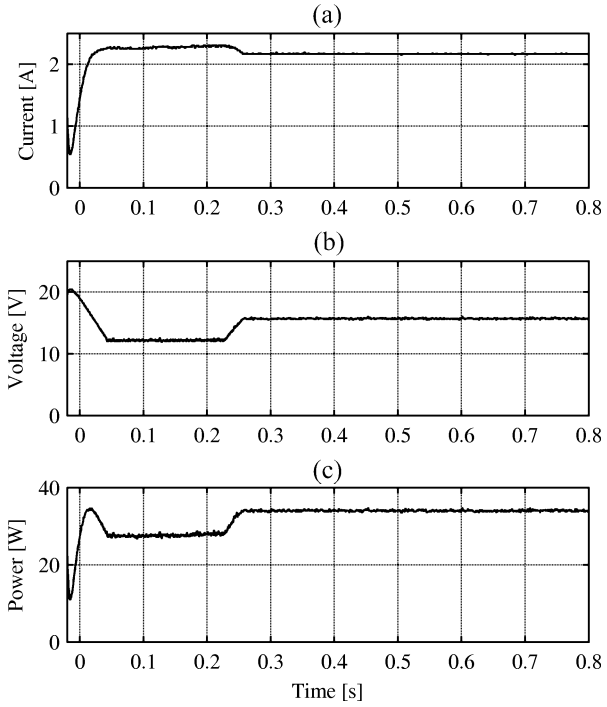

Fig. 8. (a) Current, (b) voltage, and (c) power for full, direct sun.

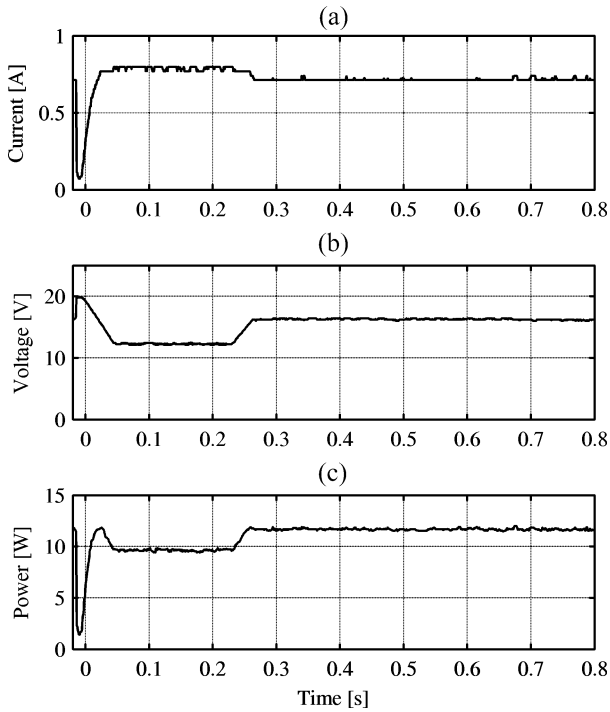

Fig. 9. (a) Current, (b) voltage, and (c) power for oblique sun.

hours, since only large-scale changes will influence its operation.

C. Experimental Results

Three operating conditions are shown in Figs. 8–10. In all three, current, voltage, and calculated power are shown. The timing is aligned so that the left boundary is near the beginning of the open-circuit mode. Voltage quickly converges to the open-circuit voltage $V_{\rm oc}$, then is driven to $0.625V_{\rm oc}$ by the CVF algorithm. This ratio (0.625), which is less than the manufacturer's specified ratio (0.80), was chosen to demonstrate the large basin of attraction for the DRCC algorithm. Measured power goes through the maximum power point, stabilizes at some lower value during the CVF mode, then converges to the maximum power point under DRCC operation. During the transient, panel current is not measured, so there is no retained information about the maximum power point. Any such information would quickly become outdated, since the insolation may change.

For Fig. 8, the panel was oriented towards the sun, and achieved 69% of rated power. This is the same operating point as in Fig. 4. For Fig. 9, the panel was turned away from the sun, to reduce the output power to 24% of rating. Numerical results for these two experiments are summarized in Table I.

Fig. 10 demonstrates dynamic tracking capability. For this test, the panel was partially shaded by a tree that was blowing in the wind. The DRCC algorithm continued to track the maximum power point. Operating point updates occurred more frequently than every 1 ms.

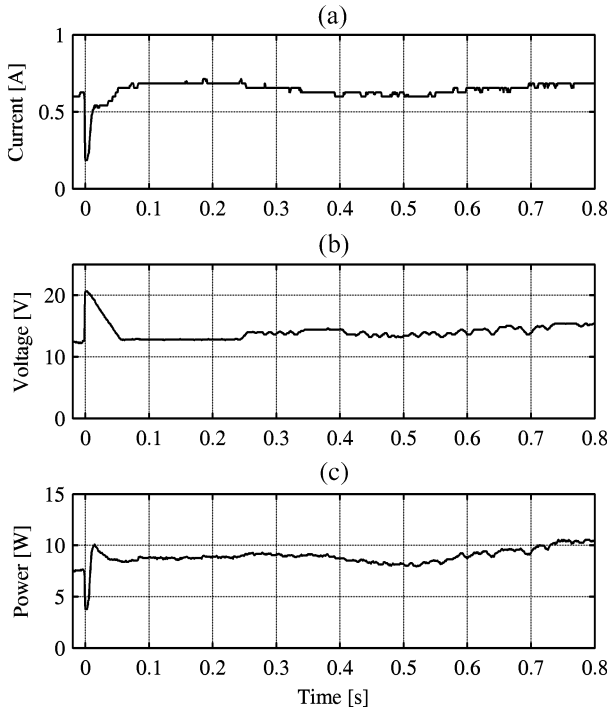

Fig. 10. (a) Current, (b) voltage, and (c) power for intermittent shading conditions.

VI. Conclusion

DRCC, a real-time digital optimization technique, was derived from the analog RCC method. For typical waveforms encountered in switching power converters, a sampling rate tied to the switching frequency can be used to implement DRCC. Stability was established. Although the new method superficially resembles conventional techniques like P&O, DRCC can reach true steady-state and uses only ripple information that is readily available in any switching power converter. Like conventional

TABLE I
SUMMARIZED EXPERIMENTAL RESULTS

Figure	Actual Maximum Power [W]	Steady-State Power [W]	Tracking Accuracy	V_{oc} [V]	Steady-State Voltage [V]	Voltage Fraction
8	34.6	34.0	98.3%	20.4	15.7	0.77
9	12.0	11.7	97.5%	19.8	16.3	0.82

RCC, DRCC can be applied to many optimization problems in power electronics.

DRCC was demonstrated in an MPPT application for photovoltaic panels. A mode-switching algorithm that used the fractional $V_{\rm OC}$ method for periodic re-initialization improved robustness and ensured that the MPPT would converge to the global maximum power point. Tracking accuracy exceeded 98% for direct insolation. An update rate of more than 1 kHz enabled the system to track maximum power on the time scale of milliseconds.

REFERENCES

[1] F. Abrahamsen, F. Blaabjerg, J. K. Pedersen, and P. B. Thoegersen, "Efficiency-optimized control of medium-size induction motor drives," *IEEE Trans. Ind. Appl.*, vol. 37, no. 6, pp. 1761–1767, Nov./Dec. 2001.

[2] M. E. H. Benbouzid and N. S. N. Said, "An efficiency-optimization controller for induction motor drives," *IEEE Power Eng. Rev.*, vol. 18, no. 5, pp. 63–64, May 1998.

[3] C. Chakraborty and Y. Hori, "Fast efficiency optimization techniques for the indirect vector-controlled induction motor drives," *IEEE Trans. Ind. Appl.*, vol. 39, no. 4, pp. 1070–1076, Jul./Aug. 2003.

[4] I. Choy, S. H. Kwon, J. Y. Choi, J. W. Kim, and K. B. Kim, "On-line efficiency optimization control of a slip angular frequency controlled induction motor drive using neural networks," in *Proc. IEEE Int. Conf. Ind. Electron., Control, Instrum.*, 1996, pp. 1216–1221.

[5] T. C. Huang and M. A. El-Sharkawi, "Induction motor efficiency maximizer using multi-layer fuzzy control," in *Proc. Int. Conf. Intell. Syst. Appl. Power Syst.*, 1996, pp. 109–113.

[6] M. W. Turner, V. E. McCormick, and J. G. Cleland, "Efficiency optimization control of AC induction motors: Initial laboratory results," Environmental Protection Agency, EPA/600/SR-96/008, May 1996.

[7] J. B. Wang and C. M. Liaw, "Indirect field-oriented induction motor drive with fuzzy detuning correction and efficiency optimisation controls," *IEE Proc. Elec. Power Appl.*, vol. 144, no. 1, pp. 37–45, Jan. 1997.

[8] J. A. A. Qahouq, H. Mao, H. J. Al-Atrash, and I. Batarseh, "Maximum efficiency point tracking (MEPT) method and digital dead time control implementation," *IEEE Trans. Power Electron.*, vol. 21, no. 5, pp. 1273–1281, Sep. 2006.

[9] V. Yousefzadeh and D. Maksimovic, "Sensorless optimization of dead times in dc-dc converters with synchronous rectifiers," *IEEE Trans. Power Electron.*, vol. 21, no. 4, pp. 994–1002, Jul. 2006.

[10] R. Balog and P. T. Krein, "Automatic tuning of coupled inductor filters," in *Proc. IEEE Power Electron. Specialists Conf.*, 2002, pp. 591–596.

[11] T. Esram and P. L. Chapman, "Comparison of photovoltaic array maximum power point tracking techniques," *IEEE Trans. Energy Convers.*, vol. 22, no. 3, pp. 439–449, Jun. 2007.

[12] P. T. Krein, "Ripple correlation control, with some applications," in *Proc. IEEE Int. Symp. Circuits Syst.*, 1999, pp. 283–286.

[13] P. Midya, "Nonlinear control and operation of dc to dc switching power converters," Ph.D. dissertation, Dept. Elect. Comput. Eng., Univ. Illinois Urbana-Champaign, Urbana-Champaign, 1995.

[14] P. Midya, P. T. Krein, and R. J. Turnbull, "Self-excited power minimizer/maximizer for switching power converters and switching motor drive applications," U.S. Patent 5 801 519, Sep. 1, 1998.

[15] P. Midya, P. T. Krein, R. J. Turnbull, R. Reppa, and J. W. Kimball, "Dynamic maximum power point tracker for photovoltaic applications," in *Proc. IEEE Power Electron. Specialists Conf.*, 1996, pp. 1710–1716.

[16] R. S. Reppa, "A maximum power point tracker for photovoltaic applications," M.S. thesis, Dept. Elect. Comput. Eng., Univ. Illinois Urbana-Champaign, Urbana-Champaign, 1996.

[17] T. Esram, "Maximum power point tracking of photovoltaic arrays using ripple correlation control," M.S. thesis, Dept. Elect. Comput. Eng., Univ. Illinois Urbana-Champaign, Urbana-Champaign, 2004.

[18] N. D. Benavides, T. Esram, and P. L. Chapman, "Ripple correlation control of a multiple-input dc-dc converter," in *Proc. IEEE Power Electron. Specialists Conf.*, 2005, pp. 160–164.

[19] D. Casadei, G. Grandi, and C. Rossi, "Single-phase single-stage photovoltaic generation system based on a ripple correlation control maximum power point tracking," *IEEE Trans. Energy Convers.*, vol. 21, no. 3, pp. 562–568, Jun. 2006.

[20] Y. H. Lim and D. C. Hamill, "Synthesis, simulation and experimental verification of a maximum power point tracker from nonlinear dynamics," in *Proc. Power Electron. Specialists Conf.*, 2001, pp. 199–204.

[21] T. Esram, J. W. Kimball, P. T. Krein, P. L. Chapman, and P. Midya, "Dynamic maximum power point tracking of photovoltaic arrays using ripple correlation control," *IEEE Trans. Power Electron.*, vol. 21, no. 5, pp. 1282–1291, Sep. 2006.

[22] D. L. Logue, "Power electronic building block applications in optimization, control, and simulation," Ph.D. dissertation, Dept. Elect. Comput. Eng., Univ. Illinois Urbana-Champaign, Urbana-Champaign, 2000.

[23] D. L. Logue and P. T. Krein, "Machine efficiency optimization using ripple correlation control," in *Proc. Appl. Power Electron. Conf.*, 2001, pp. 642–648.

[24] D. L. Logue and P. T. Krein, "Optimization of power electronic systems using ripple correlation control: A dynamic programming approach," in *Proc. IEEE Power Electron. Specialists Conf.*, 2001, pp. 459–464.

[25] D. L. Logue and P. T. Krein, "Observer-based techniques in ripple correlation control applied to power electronic systems," in *Proc. IEEE Power Electron. Specialists Conf.*, 2001, pp. 2014–2018.

[26] J. R. Wells, P. L. Chapman, and P. T. Krein, "Applications of ripple correlation control of electric machinery," in *Proc. IEEE Int. Electric Mach. Drives Conf.*, 2003, pp. 1498–1503.

[27] J. R. Wells, P. L. Chapman, and P. T. Krein, "Fundamental aspects of ripple correlation control of electric machinery," in *Proc. IEEE Power Electron. Specialists Conf.*, 2003, pp. 1659–1662.

[28] J. W. Kimball and P. T. Krein, "Continuous-time optimization of gate timing for synchronous rectification," in *Proc. Midw. Symp. Circuits Syst.*, 1996, pp. 1015–1018.

[29] J. W. Kimball and P. T. Krein, "Real-time optimization of dead time for motor control inverterse," in *Proc. IEEE Power Electron. Specialists Conf.*, 1997, pp. 597–600.

[30] J. W. Kimball and P. T. Krein, "Digital ripple correlation control for photovoltaic applicationse," in *Proc. IEEE Power Electron. Specialists Conf.*, 2007, pp. 1690–1694.

[31] J. W. Kimball, "Digital control techniques for switching power converters," Ph.D. dissertation, Dept. Elect. Comput. Eng., Univ. Illinois, Urbana, 2007.

[32] H. Patel and V. Agarwal, "MATLAB-based modeling to study the effects of partial shading on PV array characteristics," *IEEE Trans. Energy Convers.*, vol. 23, pp. 302–310, Mar. 2008.

[33] R. Balog, "Coupled Inductor: A basic filter building block, analysis, simulation and examples," M.S. thesis, Dept. Elect. Comput. Eng., Univ. Illinois Urbana-Champaign, Urbana-Champaign, 2002.

[34] R. E. Steele, *Delta Modulation*. New York: Wiley, 1975.

[35] O. Wasynczuk, "Dynamic behavior of a class of photovoltaic power systems," *IEEE Trans. Power Appl. Syst.*, vol. 102, no. 9, pp. 3031–3037, Sep. 1983.

[36] P. T. Krein and R. M. Bass, "A new approach to fast simulation of periodically switching power converters," in *Proc. Industry Applications Society Annual Meeting*, 1990, pp. 1185–1189.

[37] P. T. Krein, J. Bentsman, R. M. Bass, and B. L. Lesieutre, "On the use of averaging for the analysis of power electronic systems," *IEEE Trans. Power Electron.*, vol. 5, no. 2, pp. 182–190, Apr. 1990.

[38] J. D. Faires and B. T. Faires, *Calculus and Analytic Geometry*. Boston, MA: Prindle Weber & Schmidt, 1983.

[39] W. Cheney and D. Kincaid, *Numerical Mathematics and Computing*, 2nd ed. Belmont, CA: Wadsworth, 1985.
[40] N. D. Benavides and P. L. Chapman, "Boost converter with a reconfigurable inductor," in *Proc. IEEE Power Electron. Specialists Conf.*, 2007, pp. 1695–1700.
[41] J. J. Schoeman and J. D. van Wyk, "A simplified maximal power controller for terrestrial photovoltaic panel arrays," in *Proc. Power Electron. Specialists Conf.*, 1982, pp. 361–367.
[42] Y. Kuai, "Testing and maximum power extraction of photovoltaic panels," M.S. thesis, Dept. Elect. Comput. Eng., North Dakota State Univ., Fargo, ND, 2005.

Jonathan W. Kimball (M'96–SM'05) received the B.S. degree in electrical and computer engineering from Carnegie Mellon University, Pittsburgh, PA, in 1994, the M.S. degree in electrical engineering and the Ph.D. degree in electrical and computer engineering from the University of Illinois at Urbana-Champaign, Urbana-Champaign, in 1996 and 2007, respectively.

In 2008, he joined the Missouri University of Science and Technology (Missouri S&T), Rolla, where he is currently an Assistant Professor. He was with Motorola, Phoenix, AZ, where he designed IGBT modules for industrial applications, from 1996 to 1998. He then joined Baldor Electric, Fort Smith, AR, where he designed industrial adjustable speed drives ranging 1–150 hp. In 2003, he returned to Illinois as a Research Engineer (later a Senior Research Engineer). Later, in 2003, he cofounded SmartSpark Energy Systems, Inc., Champaign, IL, where he served as Vice President of Engineering.

Dr. Kimball is a member of Eta Kappa Nu, Tau Beta Pi, and Phi Kappa Phi. He is a licensed Professional Engineer in the State of Illinois.

Philip T. Krein (S'76–M'82–SM'93–F'00) received the B.S. degree in electrical engineering and the A.B. degree in economics and business from Lafayette College, Easton, PA, and the M.S. and Ph.D. degrees in electrical engineering from the University of Illinois, Urbana-Champaign.

He was an Engineer with Tektronix, Beaverton, OR, then returned to the University of Illinois. He currently holds the Grainger Endowed Director's Chair in Electric Machinery and Electromechanics as Director of the Grainger Center for Electric Machinery and Electromechanics. His research interests address all aspects of power electronics, machines, and drives, with emphasis on nonlinear control approaches. He published an undergraduate textbook, *Elements of Power Electronics* (Oxford Univ. Press, 1998). In 2001, he helped initiate the International Future Energy Challenge, a major student competition involving fuel cell power conversion and energy efficiency for machines. He holds 20 U.S. and four European patents.

Dr. Krein is a registered Professional Engineer in Illinois and in Oregon. He was a senior Fulbright Scholar at the University of Surrey in the United Kingdom in 1997–1998, and was recognized as a University Scholar in 1999, the Highest Research Award at the University of Illinois. He was a recipient of the IEEE William E. Newell Award in Power Electronics in 2003. In 1999–2000, he served as President of the IEEE Power Electronics Society. From 2005 to 2007, he was a Distinguished Lecturer of the IEEE Power Electronics Society.